Nuclear Engineering and Technology 50 (2018) 971–980

Contents lists available at ScienceDirect

Nuclear Engineering and Technology

journal homepage: www.elsevier.com/locate/net

Original Article

Finite element formulation and analysis of Timoshenko beam excited by transversely fluctuating supports due to a real seismic wave

Yong-Woo Kim [a, *], Seung Chan Cha [b]

[a] Department of Mechanical Engineering, Sunchon National University, 225 Jungangno, Suncheon, Jeonnam, 540-950, Republic of Korea
[b] Department of Mechanical Engineering, Graduate School, Sunchon National University, Republic of Korea

ARTICLE INFO

Article history:
Received 9 January 2018
Accepted 17 April 2018
Available online 23 April 2018

Keywords:
Finite Element Method
Quasi-static Decomposition Method
Static Component–dominated Beam
Timoshenko Beam
Time-dependent Support Motions

ABSTRACT

Using the concept of quasi-static decomposition and using three-noded isoparametric locking-free element, this article presents a formulation of the finite element method for Timoshenko beam subjected to spatially different time-dependent motions at supports. To verify the validity of the formulation, three fixed-hinged beams excited by the real seismic motions are examined; one is a slender beam, another is a stocky one, and the other is an intermediate one. The numerical results of time histories of motions of the three beams are compared with corresponding analytical solutions. The internal loads such as bending moment and shearing force at a specific time are also compared with analytic solutions. These comparisons show good agreements. The comparisons between static components of the internal loads and the corresponding total internal loads show that the static components predominate in the stocky beam, whereas the dynamic components predominate in the slender one. Thus, the total internal loads of the stocky beam, which is governed by static components, can be predicted simply by static analysis. Careful numerical experiments indicate that the fundamental frequency of a beam can be used as a parameter identifying such a stocky beam.

© 2018 Korean Nuclear Society, Published by Elsevier Korea LLC. This is an open access article under the CC BY-NC-ND license (http://creativecommons.org/licenses/by-nc-nd/4.0/).

1. Introduction

The piping in nuclear power plants would experience different motions at its ends during an earthquake if the ends or supports are connected to different main structures. The vibration of the pipe can be treated as the transverse vibration problem of a beam excited by motions at supports when the effect of fluid flow is neglected.

To solve the time-dependent boundary value problems, Mindlin and Goodman [1] developed the solution procedure called “the method of quasi-static decomposition.” They applied it to the problem of the transverse vibrations of Euler–Bernoulli beams with time-dependent boundary conditions. Since then, many investigators have applied it to the analysis of structures subjected to multiple support motions or seismic excitations via various approaches, such as time history analysis, response spectrum method of analysis, or frequency-domain spectral analysis [2–9].

Authors [4,7,10–12] formulated the finite element (FE) dynamic analysis of Euler–Bernoulli beams excited by transversely fluctuating support motions. However, a flexible connecting rod, some robotic manipulators, or some pipes between main structures in nuclear power plants are not slender beams but rather stocky ones. They are often excited by the motions transmitted from connections or supports in main structures or foundation. Thus, it is necessary to develop FE formulation based on Timoshenko beam theory (TBT). However, the investigations for FE formulation of Timoshenko beams subjected to transversely fluctuating support motions are hardly found. As for the analytic solutions of Timoshenko beam excited by transverse support motions, there are not so many articles compared with those concerning analytic solutions of Euler–Bernoulli beam, either. Lee and Lin [13] presented a solution procedure for elastically restrained nonuniform Timoshenko beams by generalizing the quasi-static decomposition method. They [14] also proposed an accurate solution procedure for the forced vibration of a pretwisted Timoshenko beam with time-dependent elastic boundary conditions by using the Mindlin–Goodman's quasi-static decomposition method. Kim [15,16] presented the procedure to obtain the responses of Timoshenko beam excited by support motions by using the expansion theorem based on the orthogonality property of eigenfunctions and also

* *Corresponding author.*
E-mail address: kyw@sunchon.ac.kr (Y.-W. Kim).

https://doi.org/10.1016/j.net.2018.04.014
1738-5733/© 2018 Korean Nuclear Society, Published by Elsevier Korea LLC. This is an open access article under the CC BY-NC-ND license (http://creativecommons.org/licenses/by-nc-nd/4.0/).

presented the analytic solutions of fixed–fixed Timoshenko beam excited by real seismic support motions.

In this study, FE formulation for the dynamic analysis of Timoshenko beam excited by spatially different, transversely fluctuating support motions is presented by using the quasi-static decomposition method. To verify the formulation, FE analysis of the three beams, which are a slender beam, a stocky beam, and an intermediate one, subjected to real seismic time histories of acceleration at supports are performed, and the results are compared with analytic solutions based on the TBT, which are obtained by using the same manner as in the studies by Kim [15] and [16]. The comparisons show good agreements. The static components of bending moment and shearing force of the three beams are also compared with the corresponding total quantities at specific instants at which maximal magnitudes of bending moment and shearing force occur during the excitation. The comparison shows that the static components of the internal loads predominate in the stocky beam, whereas the dynamic components predominate in the slender one. Through careful numerical experiments of nine groups of beams, a parameter identifying which beam is governed by static components is introduced to predict the behavior of such static component–dominated beams (or simply, SCD beam) simply by static analysis, without dynamic analysis.

2. FE formulation

The motion of Timoshenko beam with a uniform cross section in Fig. 1, which is excited by support displacements $a(t)$ and $b(t)$, is described as the following differential equations and boundary conditions.

$$\begin{cases} \rho A\ddot{y} - \kappa GA\left(y_{,xx} - \theta_{,x}\right) = 0 \\ \rho I\ddot{\theta} - EI\theta_{,xx} - \kappa GA\left(y_{,x} - \theta\right) = 0 \end{cases} \tag{1}$$

with the support motions

$$y(x,t)|_{x=0} = a(t), \quad y(x,t)|_{x=L} = b(t), \quad \theta(x,t)|_{x=0} = 0, \quad \theta_{,x}(x,t)|_{x=L} = 0 \tag{2}$$

where $y(x, t)$ is the transverse displacement and $\theta(x, t)$ is the rotational displacement of a cross section. In Eq. (1), a superimposed dot denotes a differentiation with respect to t, and the subscript of x stands for a differentiation with respect to x. EI, ρA, G, and κ denote the flexural rigidity, mass per unit length, shear modulus, and the shear coefficient, respectively. In Eq. (2), $a(t)$ and $b(t)$ denote the prescribed support displacements at the left end and the right end, respectively, and L is the length of the beam.

The free-body sketch in Fig. 2 shows the sign convention of the bending moment and the shearing force. The sign convention will be used in FE formulation later in this article to match up the sign of analytic solutions and the sign of FE solutions. Based on the TBT, the structural loads, $M(x, t)$ and $Q(x, t)$, are expressed as

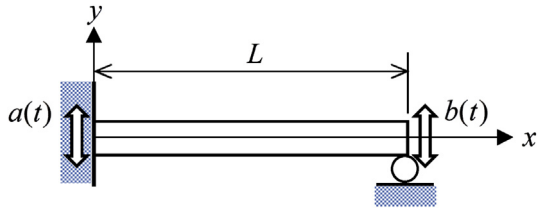

Fig. 1. A fixed-hinged beam subjected to the prescribed displacements $a(t)$ at the left support and $b(t)$ at the right support.

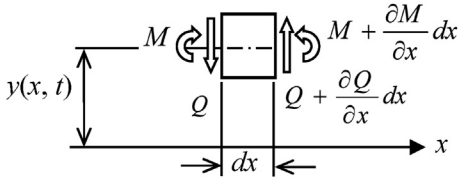

Fig. 2. Free-body sketch of a beam element of length dx.

$$\begin{aligned} M(x,t) &= EI\theta_{,x} \\ Q(x,t) &= \kappa GA\left(y_{,x} - \theta\right) \end{aligned} \tag{3}$$

According to the method of quasi-static decomposition, the total displacements $y(x, t)$ and $\theta(x, t)$ are written as the sum of a static component and a dynamic component, respectively, as follows:

$$\{u\} = \{u_s\} + \{u_d\} \tag{4}$$

where

$$\{u\} = \begin{Bmatrix} y(x,t) \\ \theta(x,t) \end{Bmatrix}, \quad \{u_s\} = \begin{Bmatrix} y_s(x,t) \\ \theta_s(x,t) \end{Bmatrix}, \quad \{u_d\} = \begin{Bmatrix} w(x,t) \\ \phi(x,t) \end{Bmatrix} \tag{5}$$

and y_s and θ_s are static displacements; w and ϕ are dynamic displacements.

2.1. Static displacements

The static displacements, y_s and θ_s, should satisfy the following static governing equations and the support conditions in Eq. (2)

$$\begin{cases} \kappa GA\left(y_{s,x} - \theta_s\right)_{,x} = 0 \\ EI\theta_{s,xx} + \kappa GA\left(y_{s,x} - \theta_s\right) = 0 \end{cases} \tag{6}$$

Solving Eq. (6) directly by using the support conditions, we can obtain the static displacements

$$y_s(x,t) = \frac{b(t) - a(t)}{\gamma + L^2/3}\left(-\frac{x^3}{6L} + \frac{x^2}{2} + \frac{\gamma}{L}x\right) + a(t) \tag{7}$$

$$\theta_s(x,t) = \frac{b(t) - a(t)}{\gamma + L^2/3}\left(-\frac{x^2}{2L} + x\right) \tag{8}$$

where $\gamma = EI/\kappa GA$. The static components of the bending moment and the shearing force are

$$M_{STATIC} = \frac{EI}{\gamma + L^2/3}\left(-\frac{x}{L} + 1\right)\cdot\{b(t) - a(t)\} \tag{9}$$

$$Q_{STATIC} = \frac{EI}{(\gamma + L^2/3)L}\cdot\{b(t) - a(t)\} \tag{10}$$

2.2. Dynamic displacements

Using Eqs. (4) to (6), we can express Eq. (1) in terms of the dynamic displacements, $w(x, t)$ and $\phi(x, t)$, as

$$\begin{cases} \rho A\ddot{w} - \kappa GA\left(w_{,xx} - \phi_{,x}\right) = g_{sy}(x,t) \\ \rho I\ddot{\phi} - EI\phi_{,xx} - \kappa GA\left(w_{,x} - \phi\right) = g_{s\theta}(x,t) \end{cases} \tag{11}$$

where

$$g_{sy}(x,t) = -\rho A \ddot{y}_s(x,t) \tag{12}$$

$$g_{s\theta}(x,t) = -\rho I \ddot{\theta}_s(x,t) \tag{13}$$

which are the inertial loadings per unit length.

The boundary conditions in Eq. (2) are also changed to the following boundary condition according to Eq. (4).

$$w(x,t)|_{x=0} = 0, \quad w(x,t)|_{x=L} = 0, \quad \phi(x,t)|_{x=0} = 0, \quad \phi_{,x}(x,t)|_{x=L} = 0 \tag{14}$$

The corresponding kinetic energy (T), deformation energy (V), and work done (W) of the beam described by Eq. (11) are

$$T = \frac{\rho I}{2}\int_0^L (\dot{\phi})^2 dx + \frac{\rho A}{2}\int_0^L (\dot{w})^2 dx \tag{15}$$

$$V = \frac{EI}{2}\int_0^L (\phi_{,x})^2 dx + \frac{\kappa GA}{2}\int_0^L (w_{,x} - \phi)^2 dx \tag{16}$$

$$W = \int_0^L g_{sy}(x,t) w dx + \int_0^L g_{s\theta}(x,t)\phi \, dx \tag{17}$$

By employing the three-noded isoparametric element in Fig. 3, we assume the dynamic displacements of an element (e) as follows

$$w^{(e)}(x,t) = [N_w]\left\{u_d^{(e)}\right\} \tag{18}$$

$$\phi^{(e)}(x,t) = [N_\phi]\left\{u_d^{(e)}\right\} \tag{19}$$

where

$$[N_w] = [N_1 \quad 0 \quad N_2 \quad 0 \quad N_3 \quad 0] \tag{20}$$

$$[N_\phi] = [0 \quad N_1 \quad 0 \quad N_2 \quad 0 \quad N_3] \tag{21}$$

The dynamic displacement vector, $\{u_d^{(e)}\}$, in Eqs. (18) and (19) is defined as

$$\left\{u_d^{(e)}\right\}^T = \left[w_1^{(e)} \quad \phi_1^{(e)} \quad w_2^{(e)} \quad \phi_2^{(e)} \quad w_3^{(e)} \quad \phi_3^{(e)}\right] \tag{22}$$

The shape functions, N_i ($i = 1, 2, 3$), in Eqs. (22) and (23) are

$$N_1 = \frac{1}{2}\left(\xi^2 - \xi\right), \quad N_2 = 1 - \xi^2, \quad N_3 = \frac{1}{2}\left(\xi^2 + \xi\right) \tag{23}$$

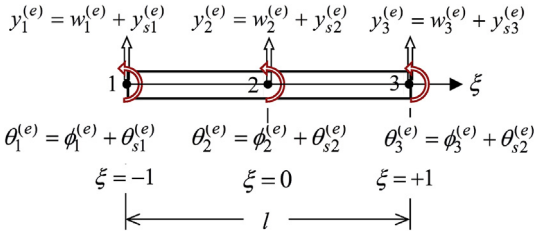

Fig. 3. Nodal variables in an element (e) of length l.

where ξ is an elemental coordinate or natural coordinate as shown in Fig. 3.

The FE equation of the beam under consideration can be obtained by introducing T, V, and W in Eqs. (15)–(17) in Hamilton's principle:

$$\left[\widehat{m}^{(e)}\right]\left\{\ddot{u}_d^{(e)}\right\} + \left[\widehat{k}^{(e)}\right]\left\{u_d^{(e)}\right\} = \left\{\widehat{g}^{(e)}\right\} \tag{24}$$

where

$$\left[\widehat{m}^{(e)}\right] = \int_{-1}^{1} \rho I [N_\phi]^T [N_\phi] |J| d\xi + \int_{-1}^{1} \rho A [N_w]^T [N_w] |J| d\xi \tag{25}$$

$$\left[\widehat{k}^{(e)}\right] = \int_{-1}^{1} EI \frac{\left[N_{\phi,\xi}\right]^T}{|J|}\frac{\left[N_{\phi,\xi}\right]}{|J|}|J| d\xi + \int_{-1}^{1} \kappa GA\left(\frac{\left[N_{w,\xi}\right]}{|J|} - [\overline{N}_\phi]\right)^T\left(\frac{\left[N_{w,\xi}\right]}{|J|} - [\overline{N}_\phi]\right)|J| d\xi \tag{26}$$

and

$$\left\{\widehat{g}^{(e)}\right\} = -\int_{-1}^{1} [N_\phi]^T g_{s\theta}^{(e)}(x,t)|J| d\xi - \int_{-1}^{1} [N_w]^T g_{sy}^{(e)}(x,t)|J| d\xi. \tag{27}$$

In Eqs. (25)–(27), $|J|$ is Jacobian determinant and $[\overline{N}_\phi]$ is defined as

$$[\overline{N}_\phi] = [0 \quad \overline{N}_1 \quad 0 \quad \overline{N}_2 \quad 0 \quad \overline{N}_3] \tag{28}$$

where $\overline{N}_i (i = 1, 2, 3)$ are

$$\overline{N}_1 = \frac{1}{2}\left(\frac{1}{3} - \xi\right), \quad \overline{N}_2 = \frac{2}{3}, \quad \overline{N}_3 = \frac{1}{2}\left(\frac{1}{3} + \xi\right) \tag{29}$$

These shape functions are the modified ones devised to avoid shear locking [17].

2.3. Total displacements

Let us introduce the following total displacement vector of an element (e),

$$\left\{u^{(e)}\right\}^T = \left[y_1^{(e)} \quad \theta_1^{(e)} \quad y_2^{(e)} \quad \theta_2^{(e)} \quad y_3^{(e)} \quad \theta_3^{(e)}\right] \tag{30}$$

The nodal displacements in Eq. (30) are depicted in Fig. 3.

Using Eq. (4), the total displacement vector is expressed as

$$\left\{u^{(e)}\right\} = \left\{u_s^{(e)}\right\} + \left\{u_d^{(e)}\right\} \tag{31}$$

where $\{u_s^{(e)}\}$ is the static displacement vector defined as

$$\left\{u_s^{(e)}\right\}^T = \left[y_{s1}^{(e)} \quad \theta_{s1}^{(e)} \quad y_{s2}^{(e)} \quad \theta_{s2}^{(e)} \quad y_{s3}^{(e)} \quad \theta_{s3}^{(e)}\right] \tag{32}$$

The entities of $\{u_s^{(e)}\}$ are easily calculated by using Eqs. (7) and (8).

Using the relation in Eq. (31), we rewrite the FE Eq. (24) in terms of the total displacement vector as

$$\left[\widehat{m}^{(e)}\right]\left\{\ddot{u}^{(e)}\right\}+\left[\widehat{k}^{(e)}\right]\left\{u^{(e)}\right\}=\left[\widehat{m}^{(e)}\right]\left\{\ddot{u}_s^{(e)}\right\}+\left[\widehat{k}^{(e)}\right]\left\{u_s^{(e)}\right\}+\left\{\widehat{g}^{(e)}\right\} \tag{33}$$

3. Numerical experiments and discussions

To validate the present formulation, we illustrate the vibration of Timoshenko beam which is initially at rest and then is excited by spatially different support motions. The first 10 s of the El Centro earthquake accelerogram (E-W component, 1940) have been used as input support motions. To model spatially different support excitations, the support accelerations, $\ddot{a}(t)$ and $\ddot{b}(t)$, are assumed as shown in Fig. 4, i.e., the time delay is assumed as 0.1 second.

For numerical tests and verifications, the three beams in Table 1 are used. The three models have the same hollow circular cross section. The input data for the beams are as follows: $\rho = 7860$ kg/m^3, $E = 200$ GPa, and Poisson's ratio $\nu = 0.3$. The shear coefficient κ [18] is

$$\kappa = \frac{6(1+m^2)^2(1+\nu)}{7+34m^2+7m^4+12\nu(1+4m^2+m^4)+4\nu(1+4m^2+m^4)} \tag{34}$$

where $m = r_i/r_o$.

We used the Newmark method with time step $\Delta t = 2.5 \times 10^{-4}$ second to integrate the FE equation of motion. Because the El Centro earthquake accelerogram consisted of discrete time history acceleration data points recorded every 0.02 second, we assumed piecewise linear accelerations between the neighboring data [16].

The convergence of FE results in terms of number of elements is shown in Fig. 5 with analytic solutions. Because the FE results converge sufficiently with 10 equal-sized FE elements as shown in Fig. 5, all the beams are discretized with 10 equal-sized FE elements throughout in this article. The analytic solutions are obtained by using the expansion theorem based on TBT, in which 20 modes are used.

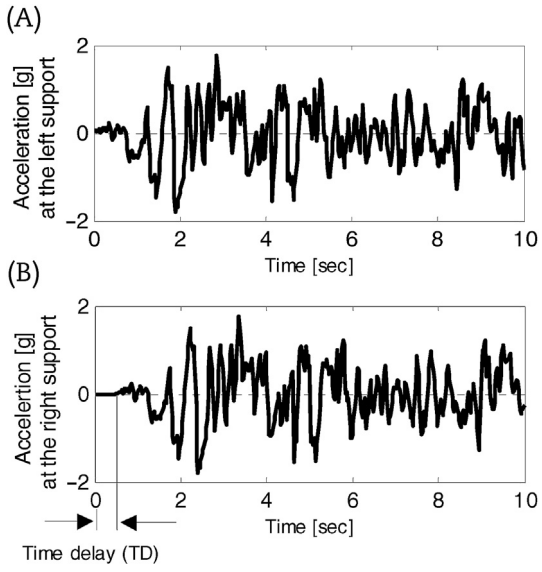

Fig. 4. The prescribed time histories of acceleration at supports. (A) $\ddot{a}(t)$ at the left end. (B) $\ddot{b}(t)$ at the right end.

Table 1
Three verification models.

Models	Beam length	Cross section
Slender beam	20 m	Hollow circular section
Intermediate beam	12 m	with outer radius $r_o = 0.1$ m
Stocky beam	2 m	and inner radius $r_i = 0.07$ m

The FE results of the three beams are compared with corresponding analytical solutions in Figs. 6–11. Figs. 6, 8, and 10 show the linear motions (y, $\dot{y}$, and $\ddot{y}$) and the angular motions (θ, $\dot{\theta}$, and $\ddot{\theta}$) at the midpoint of the beams. These figures show that the FE results of motions agree with the corresponding analytical solutions based on the TBT.

The total quantities of displacement, rotation angle, bending moment, and shearing force along the beam length at specific instants are plotted in Figs. 7, 9, and 11, together with analytic solutions and static quantities. The specific times are the instants at which the maximal magnitude of shearing force occurs during the forced vibration. The maximal magnitude of the shearing force occurs at $t = 6.39$ second in the slender beam, $t = 8.44$ second in the intermediate beam, and $t = 2.19$ second in the stocky beam. The FE results of the total quantities show good agreements with the corresponding analytic solutions. The static components of displacements y_s and θ_s are calculated by Eqs. (7) and (8), and the static component of internal loads M_{STATIC} and Q_{STATIC} are calculated by Eqs. (9) and (10), respectively. Comparing the static components and the corresponding total quantities (FEM or Analytic) in Figs. 7, 9, and 11, we can observe the following facts:

- The maximal magnitudes of $|y_{total} - y_s|$ and $|\theta_{total} - \theta_s|$ become smaller as the beam length decreases, and the static displacements y_s and θ_s of the stocky beam approach the total displacement and the total rotation, respectively.
- The values of M_{STATIC} and Q_{STATIC} go near the corresponding total quantities M_{total} and Q_{total} respectively, as the beam length decreases. In the slender beam, the magnitudes of M_{STATIC} and Q_{STATIC} are very small compared with the magnitudes of the corresponding total quantities. But, in the stocky beam, the static parts of the internal loads are very close to those of the total loads.

From the above observations, we see that the displacements and internal loads of the stocky beam are governed by their static components, whereas those of the slender beam are governed by dynamic components. Therefore, the behavior of SCD beam can be predicted simply by static analysis, without dynamic analysis. Thus, the following measures to identify SCD beam are introduced.

$$R_{MM} = \frac{M_{STATIC}}{M_{total}} \text{ and } R_{QQ} = \frac{Q_{STATIC}}{Q_{total}} \tag{35}$$

where R_{MM} is calculated at the location and time the maximal magnitude of $|M_{total}|$ occurs and R_{QQ} at the location and instant the maximal magnitude of $|Q_{total}|$ occurs during the support fluctuations. It is expected that these measures approach 1 for SCD beams and go to zero for dynamic component–dominated beams.

According to the author's experience, the higher the fundamental frequency (Ω) of a beam is and the smaller the slenderness ratio ($s = L/r$, where r is a radius of gyration) is, the more dominant the static components become. Thus, if there exists a certain suitable parameter to identify the SCD beam, the feature of the SCD beam can be used in a structural design. To find such a suitable parameter, numerical experiments for the nine groups of fixed-hinged beams in Table 2 are performed by using the entire El Centro

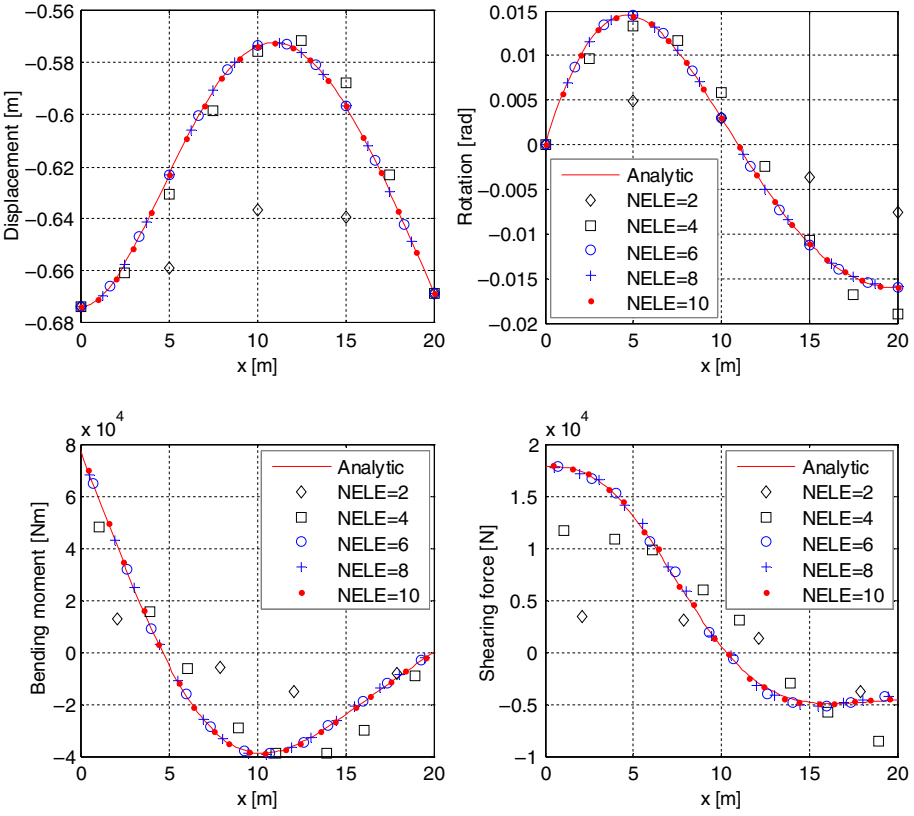

Fig. 5. Convergence of displacement, rotation, bending moment, and shearing force of the slender beam in terms of number of elements when $t = 6.39$ second.

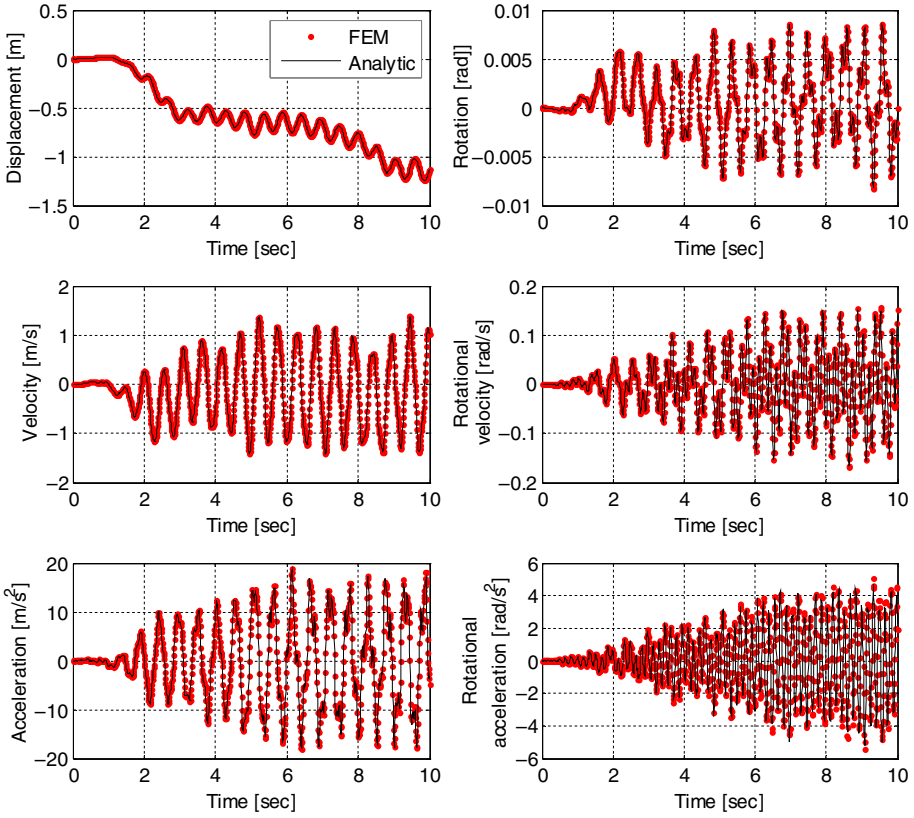

Fig. 6. Time histories of motions of the slender beam at the midpoint, $x = 10$ m.
FEM, finite element method.

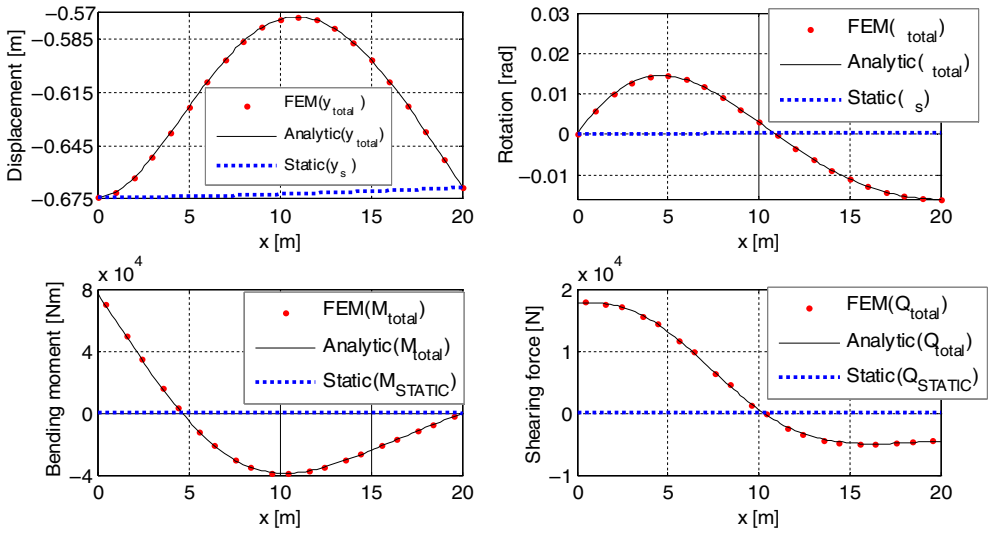

Fig. 7. Displacement, rotation, bending moment, and shearing force of the slender beam when $t = 6.39$ second.
FEM, finite element method.

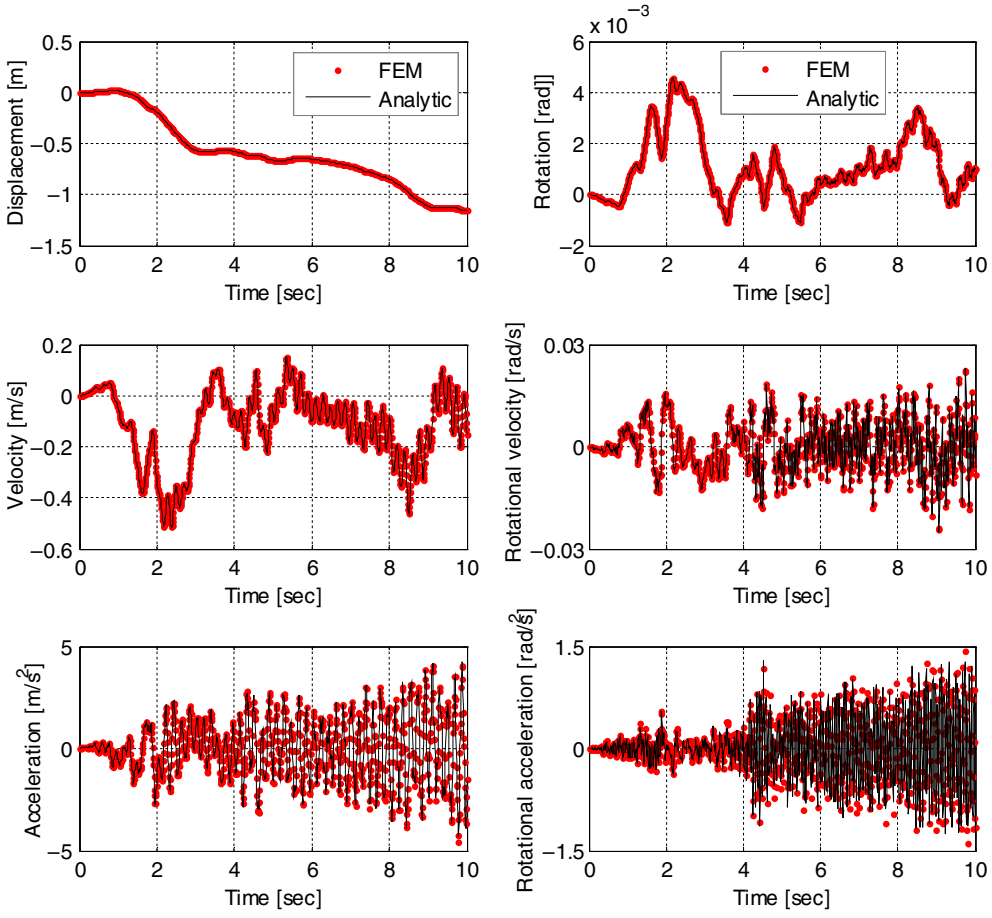

Fig. 8. Time histories of motions of the intermediate beam at the midpoint, $x = 6$ m.
FEM, finite element method.

earthquake accelerogram (E-W component, 1940) as input support motions. The shear coefficients of hollow circle, solid circle, and thin-walled hollow circle in Table 2 are calculated by Eq. (34) and those of rectangular sections are calculated by the following equation [18].

$$\kappa = \frac{10(1+\nu)}{12+10\nu-\frac{180\nu^2}{1+\nu}\left(\frac{b}{h}\right)^4\sum_{n=1}^{\infty}\frac{n\pi-(b/h)\tanh(n\pi h/b)}{(n\pi)^5}} \tag{36}$$

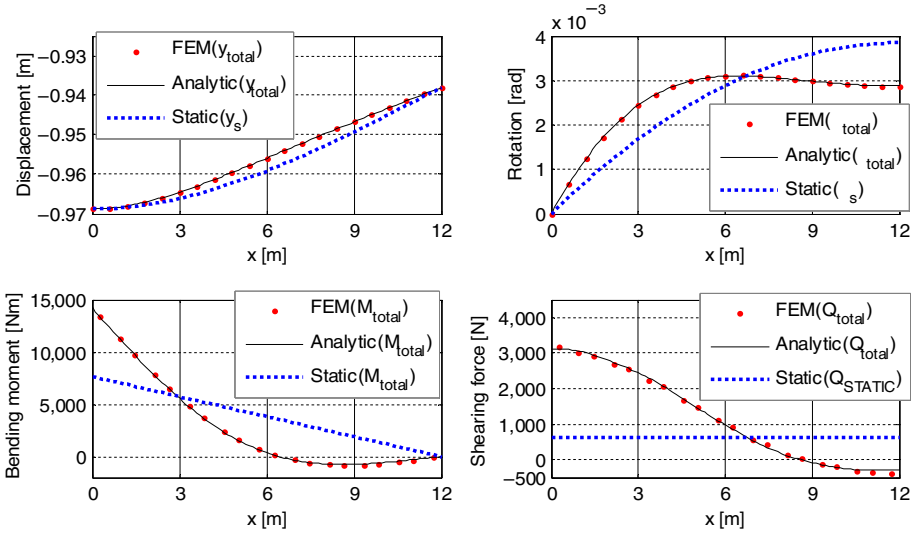

Fig. 9. Displacement, rotation, bending moment, and shearing force of the intermediate beam when $t = 8.44$ second.
FEM, finite element method.

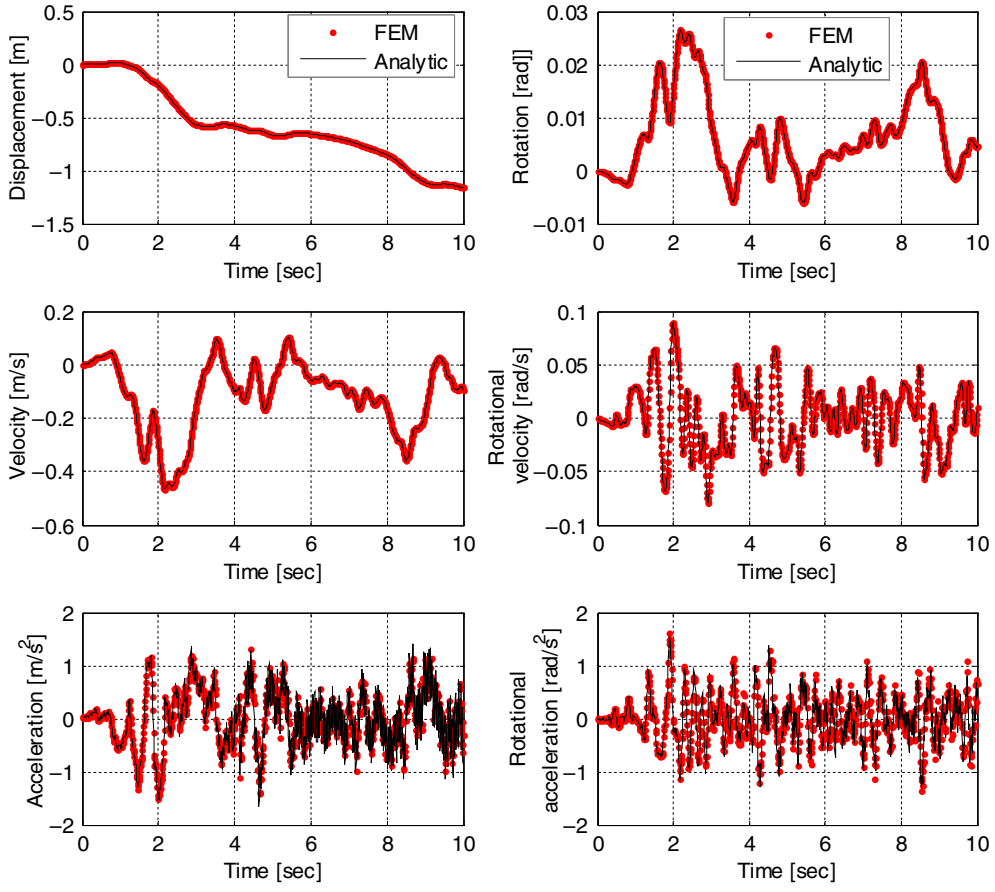

Fig. 10. Time histories of motions of the stocky beam at the midpoint, $x = 1$ m.
FEM, finite element method.

where b and h denote width and height of a rectangular section, respectively.

The measures of R_{MM} and R_{QQ} in terms of 1/s and fundamental frequency of beams (Ω_{TBT}) are plotted in Figs. 12 and 13, respectively. Fig. 12 does not show a consistent relation between the measures and 1/s in the entire nine groups although the measures of each group increase as 1/s increases. Thus, the parameter of 1/s is not a suitable one for identification of the SCD beam. Fig. 13 shows more consistent relations between the measures and fundamental frequency (Ω_{TBT}) than the relations in Fig. 12. The frequencies (Ω_{TBT}) in Fig. 13 are obtained by FE eigenvalue analysis based on the TBT.

From Fig. 13, following two facts can be observed; one is that $R_{MM} \geq 0.9$ when $\Omega_{TBT} > 65$ rad/sec, and the other one is that $R_{QQ} \geq 0.9$ when $\Omega_{TBT} > 100$ rad/sec. Thus, the fundamental frequency

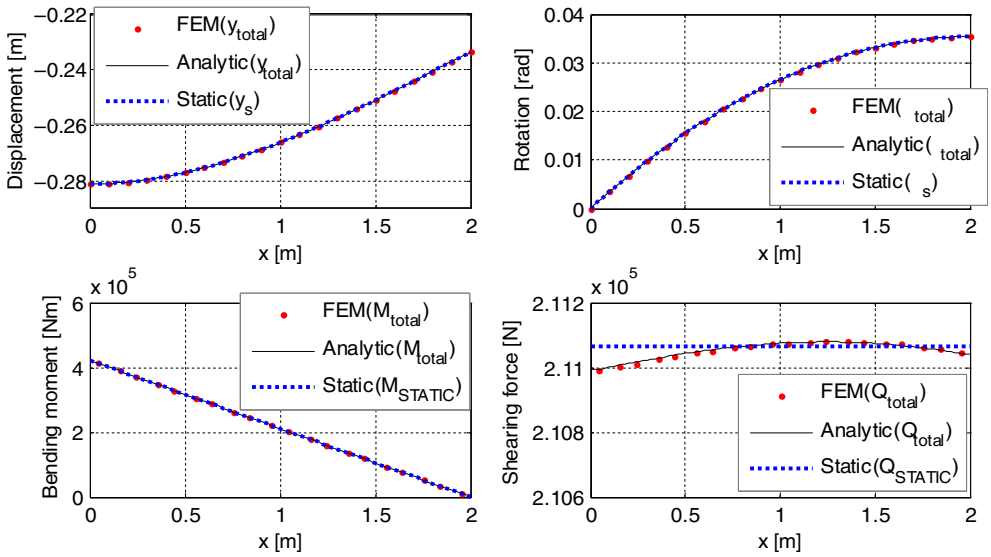

Fig. 11. Displacement, rotation, bending moment, and shearing force of the stocky beam when $t = 2.19$ second.
FEM, finite element method.

Table 2
Nine groups of fixed-hinged beams for numerical experiments.

Materials	Designations	Cross section	Beam length L [m]	Input data
Steel beams	S, HolCir	Hollow circle; $r_o = 0.1$ m, $r_i = 0.07$ m, $\kappa = 0.592212$	4.0, 4.5, 5.0, 5.5, 6.0, 6.5, 7.0, 7.5, 8.0, 8.5, 9.0, 9.5, 10.0, 12.0, 14.0, 16.0, 18.0, 20.0	$E = 200$ GPa, $\rho = 7860$ kg/m^3, $\nu = 0.3$, TD = 0.1 s
	S, SolCir	Solid Circle; $r_o = 0.1$ m, $r_i = 0.0$ m, $\kappa = 0.925182$		
	S, ThinHolCir	Thin walled hollow circle; $r_o = 0.1$ m, $r_i = 0.09$ m, $\kappa = 0.567651$		
Copper beams	C, HolCir	Hollow circle; $r_o = 0.1$ m, $r_i = 0.07$ m, $\kappa = 0.592212$		$E = 120$ GPa, $\rho = 8900$ kg/m^3, $\nu = 0.34$, TD = 0.1 s
	C, SolCir	Solid Circle; $r_o = 0.1$ m, $r_i = 0.0$ m, $\kappa = 0.925182$		
	C, ThinHolCir	Thin-walled hollow circle; $r_o = 0.1$ m, $r_i = 0.09$ m, $\kappa = 0.567651$		
Steel beams	S, Rec (h = 0.01 m)	Rectangle; $b \times h = 0.01$ m $\times$ 0.01 m, $\kappa = 0.872272$	0.9, 1.0, 1.1, 1.2, 1.3, 1.4, 1.5, 1.6, 1.7, 1.8, 1.9, 2.0, 2.5, 3.0, 4.0	$E = 200$ GPa, $\rho = 7860$ kg/m^3, $\nu = 0.3$, TD = 0.1 s
	S, Rec (h = 0.05 m)	Rectangle; $b \times h = 0.01$ m $\times$ 0.05 m, $\kappa = 0.866679$	2.0, 2.5, 3.0, 3.5, 4.0, 4.5, 5.0, 5.5, 6.0, 6.5 7.0, 7.5, 8.0, 9.0, 10.0	
	S, Rec (h = 0.10 m)	Rectangle; $b \times h = 0.01$ m $\times$ 0.10 m, $\kappa = 0.866667$	3.0, 3.5, 4.0, 4.25, 4.5, 4.75, 5.0, 5.5, 6.0, 6.5, 7.0, 8.0, 9.0, 10.0, 14.0	

TD, time delay.

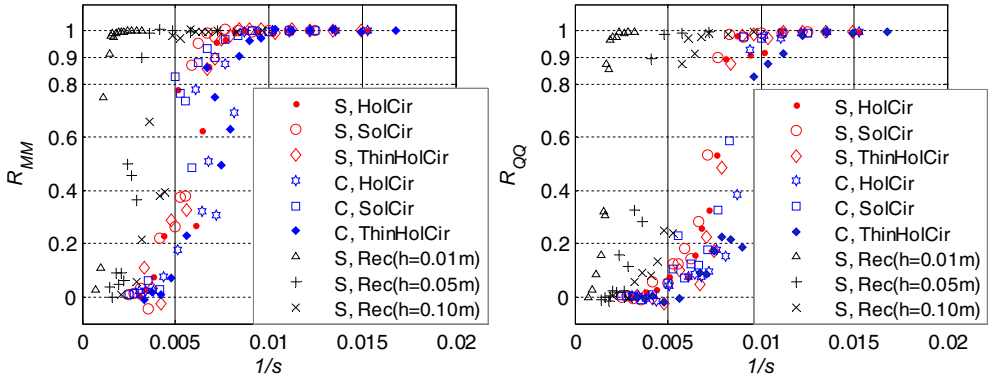

Fig. 12. R_{MM} and R_{QQ} in terms of 1/s.

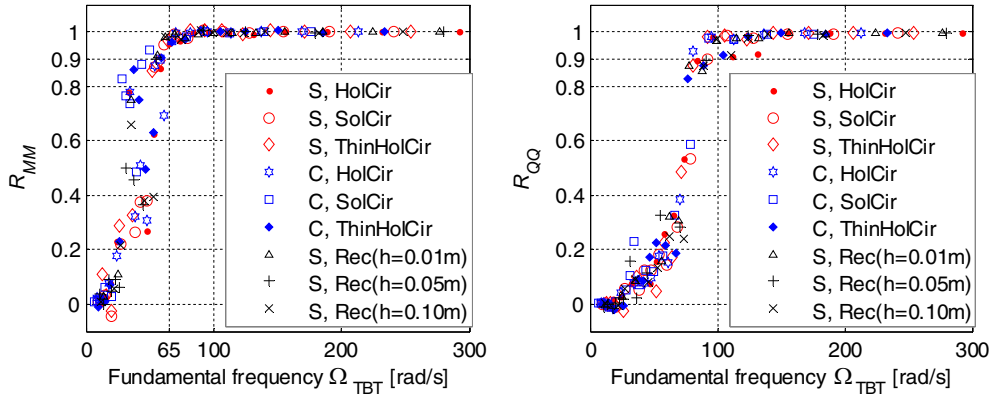

Fig. 13. R_{MM} and R_{QQ} in terms of the fundamental frequency, Ω_{TBT}.

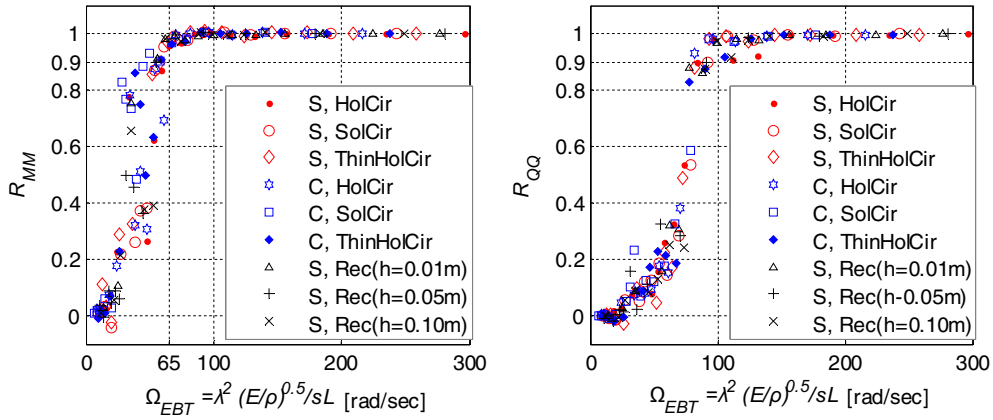

Fig. 14. R_{MM} and R_{QQ} in terms of the fundamental frequency, Ω_{EBT}.

should be greater than 100 rad/sec for both R_{MM} and R_{QQ} to be greater than 0.9, simultaneously. Based on the numerical results, the SCD beam can be defined as a beam with fundamental frequency greater than 100 rad/sec.

In Fig. 12, the values of 1/s of the most beams are less than 0.01. This implies that most of the beams with fundamental frequencies less than 100 rad/sec are slender ones. Thus, the fundamental frequency of Euler–Bernoulli beam (Ω_{EBT}) can be used instead of the fundamental frequency of Timoshenko beam (Ω_{TBT}). The fundamental frequency based on Euler–Bernoulli beam theory is given by

$$\Omega_{EBT} = \lambda^2 \frac{\sqrt{E/\rho}}{sL} \tag{37}$$

where $\lambda = 3.92660231$ for the fixed-hinged beam [19]. Using the Ω_{EBT}, we replot Fig. 13 in Fig. 14. Comparing Fig. 14 with Fig. 13 shows that it is possible to identify the SCD beams by Ω_{EBT}. Using Ω_{EBT} in Eq. (37) is more convenient than using the fundamental frequency of Timoshenko beam because Ω_{EBT} can be calculated easily by the basic data, E, ρ, s, and L, without eigenvalue analysis.

In addition, it is noteworthy that the magnitudes of the bending moment and shearing force of the SCD beam are nearly proportional to the magnitude of the difference of support motions, i.e., $|a(t)\text{-}b(t)|$, and that the maximal magnitudes of the structural loads occur at the instant that the difference of support motions is maximum during support excitation, which can be recognized clearly from Eqs. (9) and (10) [16].

In summary, once we know the fundamental frequency of fixed-hinged beam subjected to transversely fluctuating support motions, we can recognize whether the beam is the SCD beam or not by using its fundamental frequency. If a beam belongs to the SCD beam, it is possible to analyze the beam simply by static analysis without dynamic analysis and to predict when and where maximal bending moment and shearing force occur. To generalize the fundamental frequency as the parameter identifying the SCD beam, further numerical experiments on other beams with different boundary conditions are required.

4. Conclusions

With the three-noded isoparametric Timoshenko beam element, the formulation for dynamic analysis of Timoshenko beam excited by spatially different support motions is presented. Three kinds of fixed-hinged beams subjected to real seismic motions at supports are illustrated to check the validity of the present FE formulation; one is a slender beam, another is a stocky beam, and the other is an intermediate beam. The FE results of the three beams show good agreements with the corresponding analytic solutions. Examination of the FE results of the three beams shows an interesting fact that the static components predominate in the stocky beam, whereas the dynamic components predominate in the slender one. Thus, it is necessary to introduce the concept of SCD beam to use its feature in a structural analysis and design. Through numerical experiments of the fixed-hinged beams with various cross sections and lengths, it is shown that the fundamental

frequency can be used as a suitable parameter to identify the SCD beam.

Conflicts of interest

The authors have no conflicts of interest to declare.

References

[1] R.D. Mindlin, L.E. Goodman, Beam vibrations with time-dependent boundary conditions, J. Appl. Mech. ASME 17 (1950) 377–380.
[2] S.F. Masri, Response of beam to propagating boundary excitation, Earthq. Eng. Struct. Dynam. 4 (1976) 497–509.
[3] A.M. Abdel-Ghaffar, J.D. Rood, Simplified earth-quake analysis of suspension bridge towers, J. Eng. Mech. Div. ASCE 108 (EM2) (1982) 291–302.
[4] P. Léger, I.M. Idé, P. Paultre, Multiple-support seismic analysis of large structures, Comput. Struct. 36 (6) (1990) 1153–1158.
[5] R.W. Clough, J. Penzien, Dynamics of Structures, second ed., McGraw-Hill, Singapore, 1993.
[6] A.K. Chopra, Dynamics of Structures: Theory and Application to Earthquake Engineering, Prentice Hall, USA, 1995.
[7] J.T. Chen, H.-K. Hong, C.S. Yeh, S.W. Chyuan, Integral representations and regularizations for a divergent series solution of a beam subjected to support motions, Earthq. Eng. Struct. Dynam. 25 (1996) 909–925.
[8] Y.H. Zhang, Q.S. Li, J.H. Lin, F.W. Williams, Random vibration analysis of long-span structures subjected to spatially varying ground motions, Soil Dynam. Earthq. Eng. 29 (2009) 620–629.
[9] T.K. Datta, Seismic Analysis of Structures, John Wiley & Sons (Asia) Pte Ltd, Singapore, 2010.
[10] Y.-W. Kim, M.J. Jhung, Moving support elements for dynamic finite element analysis of statically determinate beams subjected to support motions, Trans. Korean Soc. Mech. Eng. A 37 (4) (2013) 555–567.
[11] Y.-W. Kim, Finite element formulation for earth-quake analysis of single-span beams involving forced deformation caused by multi-support motions, J. Mech. Sci. Technol. 29 (2) (2015) 461–469.
[12] Y.-W. Kim, S.Y. Lee, FE dynamic analysis using moving support element on multi-span beams subjected to support motions, Mod. Mech. Eng. 5 (2015) 112–121.
[13] S.Y. Lee, S.M. Lin, Non-uniform Timoshenko beams with time-dependent elastic boundary conditions, J. Sound Vib. 217 (9) (1998) 223–238.
[14] S.M. Lin, S.Y. Lee, The forced vibration and boundary control of pretwisted Timoshenko beams with general time dependent elastic boundary conditions, J. Sound Vib. 251 (1) (2001) 69–90.
[15] Y.-W. Kim, Dynamic analysis of Timoshenko beam subjected to support motions, J. Mech. Sci. Technol. 30 (2) (2016) 4167–4176.
[16] Y.-W. Kim, Analytic solution of Timoshenko beam excited by real seismic support motions, Struct. Eng. Mech. 62 (2) (2017) 247–258.
[17] G. Prathap, R. Babu, Field-consistent strain interpolations for the quadratic shear flexible beam element, Int. J. Numerical Methods Eng. 23 (1986) 1973–1984.
[18] J.R. Hutchinson, Shear coefficients for Timoshenko beam theory, J. Appl. Mech. 68 (2001) 87–92.
[19] R.D. Blevins, Formulas for Natural Frequency and Mode Shape, Van Nostrand Reinhold, NewYork, 1979.